Dalton Transactions

PAPER

View Article Online
View Journal | View Issue

Cite this: *Dalton Trans.*, 2018, **47**, 758

High-valent nitridorhenium(v) complexes containing PNP ligands: implications of ligand flexibility†

Nikola S. Lambic, Roger D. Sommer and Elon A. Ison *

Received 25th September 2017,
Accepted 7th December 2017

DOI: 10.1039/c7dt03615a

rsc.li/dalton

The synthesis of (PNP)Re(N)X (PNP = [2-P(CHMe$_2$)$_2$-4-MeC$_6$H$_3$]$_2$N, X = Cl and Me) complexes is described. The methylnitridorhenium complex **3** was found to react differently with CO and isocyanides, leading to the isolation of a Re(v) acyl complex **4** and an isocyanide adduct **6**. Two parallel pathways were observed for the reaction of **3** with CO: (1) CO inserts into the Re–Me bond to afford **4**, and (2) **3** isomerizes by distortion of the aryl backbone of the PNP ligand to afford the isomer **3′**. This is followed by the reaction of **3′** with CO to afford the tricarbonyl complex **5**, which was fully characterized. The contrasting reaction of **3** with 2,6-dimethylphenyl isocyanide lends further support for the proposed isomerization pathway. DFT (M06) calculations suggest that insertion of CNR into the Re–Me bond (27.2 kcal mol^{-1}) is inaccessible at room temperature. Instead the substrate adds to the metal center *via* the most accessible face *i.e. syn* to the rhenium–nitrido bond, to afford **6**. The addition of CO to isomer **3′** is proposed to proceed with a similar mechanism to 2,6-dimethylphenyl isocyanide.

Introduction

High-valent rhenium complexes with oxo and imido ligands are well established in catalysis.[1] In contrast, the analogous chemistry of complexes with nitrido ligands is less developed.[2] Recently, our group has shown that the *trans* influence of the oxo group in square pyramidal oxorhenium complexes affects the outcome of many fundamental organometallic reactions with these species.[3] We were interested in exploring the *trans* influence of isoelectronic nitrido ligands in analogous complexes in order to: (1) assess the effect of changing the heteroatom in the rhenium complexes that contain a multiple bond and (2) consequently gain insight from this understanding for the design of new catalysts that feature high-valent rhenium complexes.

In order to synthesize neutral nitrido complexes analogous to the previously reported oxorhenium species it was necessary to incorporate a monoanionic chelating ligand. Recently, PNP pincer ligands have been utilized in many catalytic and stoichiometric reactions.[4] However, the use of PNP complexes with rhenium in catalysis has been relatively limited, though these complexes have been utilized in stoichiometric reactions.[5] In this manuscript, we describe the synthesis of complexes of the form (PNP)Re(N)X, (where PNP = [2-P(CHMe$_2$)$_2$-4-MeC$_6$H$_3$]$_2$N and X = Cl, and Me). The non-rigidity of the PNP ligand[5e,6] results in conformational isomerization of the resultant rhenium complex. In carbonylation reactions, these conformational changes ultimately compete with CO insertion. Given the prevalence of the PNP ligand framework in transition metal chemistry,[4a,5g,7] it is suggested that the observed non-rigidity may play an important role in the reactivity of complexes incorporating this ligand.

Results and discussion

Synthesis of (PNP)Re(N)X complexes

Heating a CH_2Cl_2 solution of the previously reported complex, *trans* (Ph$_3$P)$_2$Re(N)Cl$_2$,[2i] with one equivalent of **1** and Et$_3$N afforded (PNP)Re(N)Cl, **2**, in moderate yield (51%) as an orange powder (Scheme 1). In this reaction, the equivalent of Et$_3$N serves as an external base to neutralize an equivalent of HCl. The resulting salt Et$_3$N·HCl was easily be removed by washing the isolated powder with methanol.

Complex **2** was characterized by NMR spectroscopy, elemental analysis and mass spectrometry. While the X-ray crystal structure was obtained, disorder around the rotating diarylamido backbone (*vide infra*) prevented satisfactory refinement. Characteristic resonances for the aromatic signals of the PNP

Department of Chemistry, North Carolina State University, 2620 Yarbrough Drive, Raleigh, North Carolina 27695-8204, USA. E-mail: eaison@ncsu.edu

†Electronic supplementary information (ESI) available: X-ray experimental for **4** and **6**. CIF files. NMR and IR spectra. Full Gaussian reference and XYZ files. CCDC 1588815, 1547643 and 1547644. For ESI and crystallographic data in CIF or other electronic format see DOI: 10.1039/c7dt03615a

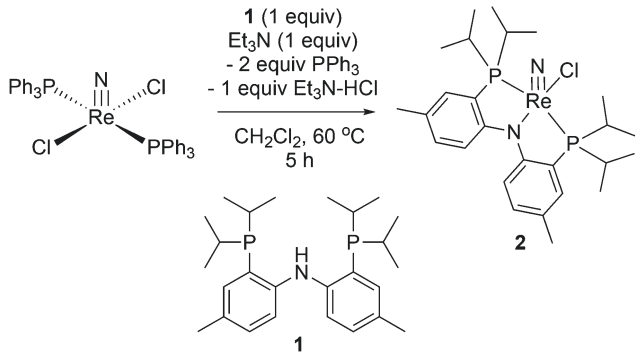

Scheme 1 Synthesis of (PNP)Re(N)Cl, **2**.

ligand are observed in the ^{1}H NMR spectrum of **2**. The isopropyl group is observed as two separate methine signals at 2.91 and 2.58 ppm and four separate methyl signals. Similar structural features of the diisopropyl fragments were observed in the previously reported oxo analogs (DippDAP)Re(O)X, (DippDAP = 2,6-diisopropylphenyl-bisaminomethylpyridine; X = H, Cl, Me, Ph) which feature similar coordination environments at rhenium.[8]

By ^{31}P NMR spectroscopy, one signal is observed at 51.9 ppm, confirming that there is a plane of symmetry through the nitrogen, rhenium and chlorine atoms, which results in both phosphorus groups in chemically equivalent environments. The nitridorhenium methyl complex, (PNP)Re(N)Me, **3**, was synthesized by heating a THF solution of **2** with five equivalents of MeMgBr (Scheme 2).

Complex **3** was isolated as a red powder and was characterized by ^{1}H and ^{31}P NMR spectroscopy, elemental analysis and X-ray crystallography (see ESI†). A similar splitting pattern to **2** was observed in the ^{1}H NMR spectrum for the aromatic and isopropyl groups. In addition, a new triplet at 1.82 ppm (J = 4.7 Hz) was assigned to the methyl ligand. This is consistent with the coupling of protons from the methyl group to two identical phosphorus atoms. The chemical shift for the methyl ligand is in good agreement with similar isoelectronic oxo complexes.[3b–d,8] To further confirm the presence of the rhenium–methyl bond in **3**, the deuterated analog, **3-d**, was synthesized from CD_3MgBr. The spectrum for **3-d** was similar to **3**, however, the signal for the methyl ligand was not observed in the ^{1}H NMR spectrum.

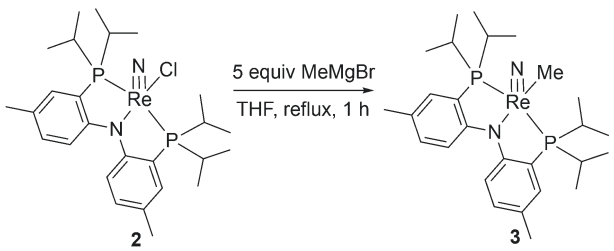

Scheme 2 Synthesis of (PNP)Re(N)Me, **3**.

Reactivity of 3 with CO and CNAr

Complex **3** reacts with CO at low temperatures and pressures (1 atm, 298 K) to afford the acyl species **4** in 35% yield. This yield can be significantly improved by briefly heating the reaction mixture at 80 °C to afford complex **4** in 64% isolated yield. In addition to **4**, complex, **5**, assigned as (PNP)Re(CO)$_3$ was also formed, (*vide infra*), over several days, *via* the further reduction of the metal center. The acetyl complex **4** was characterized by ^{1}H and ^{31}P NMR spectroscopy, FT-IR spectroscopy, X-ray crystallography and elemental analysis. By ^{1}H NMR spectroscopy, protons on the methyl group were observed as a singlet at 2.95 ppm. The loss of coupling to the phosphorus atoms is consistent with the insertion of CO into the Re–Me bond in **3**. Other resonances are consistent with previously reported PNP complexes.[5f] A slight shift of the ^{31}P NMR signal was observed for **4** (57.7 ppm) compared to **3** (54.6 ppm) (Scheme 3).

X-ray quality crystals were obtained by the slow evaporation overnight of a methylene chloride solution of **4** at room temperature. The thermal ellipsoid plot for **4** is displayed in Fig. 1. The relatively short Re1–N1 bond is indicative of a rhenium–nitrogen triple bond.[9] Furthermore, Re1–C1 bond length is shorter than expected and possesses significant carbene character resulting from the π donation from the metal nonbond-

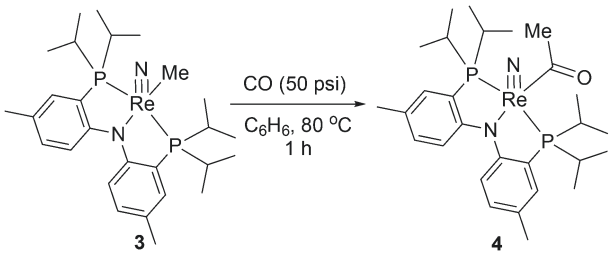

Scheme 3 Synthesis of **4**.

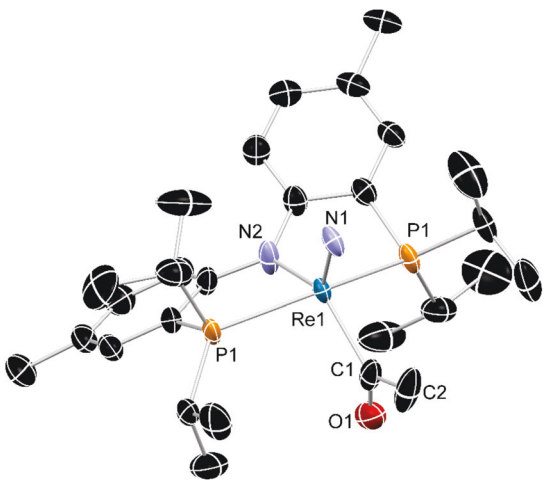

Fig. 1 X-ray crystal structure of **4**. Ellipsoids are at 50% probability level. Selected bond lengths (Å): Re1–N1 1.673(6); Re1–C1 2.016(7); C1–O1 1.250(9); C1–C2 1.524(11); Re1–P1 2.463(0); Re1–N2 2.135(4).

ing d_{xy} orbital into the antibonding orbital of the acyl ligand.[10] Similar behavior was observed for acyl complexes of the oxo analogs that incorporate diamidopyridine (DAP) and diamidoamine (DAAm) ligands.[3b,d,11]

The assignment of the C═O stretch for **4** by FTIR spectroscopy was not obvious. Thus, DFT calculations (M06)[12] were performed to assist in this assignment.[13] By DFT, the C═O stretch for the acyl ligand was identified at 1520 cm^{-1}. The calculated FTIR spectrum is in excellent agreement with the spectrum obtained experimentally (see ESI†). The low value of the C═O stretch is consistent with increased donation from the nitrido ligand to the metal center. Increased electron density at the metal results in increased π-backbonding to the π* orbital of the C═O fragment. In comparison, the acyl stretches for similar isoelectronic oxo species, are observed at 1587 cm^{-1} for complexes that incorporate the diamidoamine (DAAm)[3d] ligands, and 1620 cm^{-1} for complexes bearing weakly donating 2-mercaptoethylsulfide (SSS) ligands.[3a]

Characterization of 5

In order to further elucidate the structure of **5** additional reactions of **3** with CO were examined (Scheme 4). Exposure of **3** to a CO atmosphere at 80 °C for 24 h results in quantitative formation of **5**. This reaction presumably releases a mixture of reactive methylisocyanate and acetyl isocyanate, which undergo reactivity with exogenous water to afford methylamine and acetamide respectively. The details of this transformation, and the evidence for isocyanate formation are discussed later.

A green powder was obtained by removing **5** *via* precipitation with pentane. Three sets of terminal CO stretches at 2018 and 2003 cm^{-1} (weak) and 1909 and 1887 cm^{-1} (s) were observed by FTIR spectroscopy (see ESI†). The intensity of these stretches suggests a *trans* disposition for the two carbonyl ligands.[14] The two sets of carbonyl ligands are attributed to two conformations imposed by the rotation of the PNP aryl rings around the nitrogen linker (*vide infra*). Slow evaporation of a reaction mixture afforded X-ray quality crystals of **5** (see ESI†) a tricarbonyl complex previously reported by Ozerov and co-workers[5k] that is consistent with the FTIR data. The structure features a meridional arrangement of carbonyl ligands, typical for other rhenium complexes bearing this PNP ligand. The distortion around Ar–N–Ar moiety is 27°, which is similar to the nitride species **4**. In order to further confirm the structure of **5**, the complex was synthesized independently according to Scheme 5. The spectroscopic characteristics of **5** synthesized *via* this route are identical to that observed from the carbonylation of **3**.

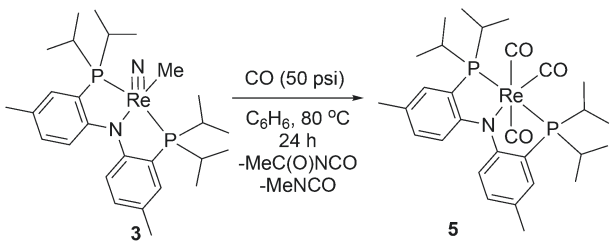

Scheme 4 Formation of **5** from **3**.

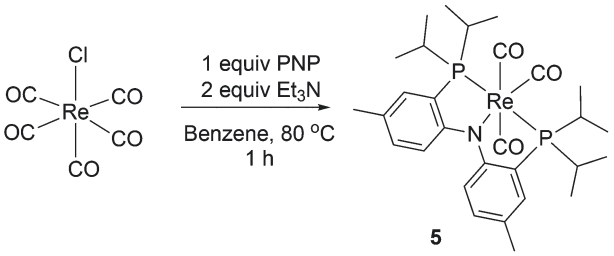

Scheme 5 Independent synthesis of **5**.

Mechanism for the carbonylation of 3

In order to evaluate the mechanism for the reaction of **3** with CO, room temperature kinetic studies were performed. The time profile for the carbonylation of **3** is shown in Fig. 2. As depicted in this figure, the formation of **4** proceeded exponentially to approximately 35% yield. This yield was also consistent with the isolated yield for **4** at room temperature.

From Fig. 2, **3** decays exponentially as well as the total rhenium concentration. A plot of k_{obs} for the decay of **3** *versus* CO pressure (Fig. 3) is linear (slope = 1.1×10^{-4} min^{-1} psi^{-1}) with a significant intercept (intercept = 3.2×10^{-3} min^{-1}). The exponential decay of the total rhenium concentration is consistent with the formation of another rhenium species in addition to **4**. As suggested above, this species has been assigned as an intermediate that eventually leads to the Re(I) tricarbonyl species **5**.

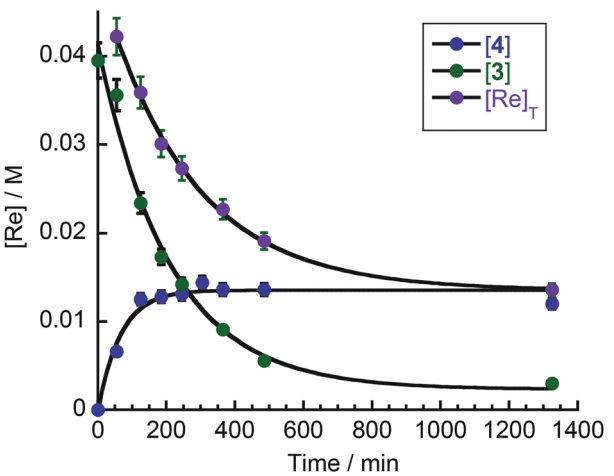

Fig. 2 Time profile for carbonylation of **3** in the presence of CO. Conditions: [**3**] = 0.04 M in benzene-d_6, *p*CO = 20 psi. Conversions monitored by ^{1}H NMR spectroscopy in a J. Young tube with mesitylene as the internal standard. Rate constants (min^{-1}): **4** = 1.5(3) × 10^{-2}; **3** = 4.8(6) × 10^{-3}; $[Re]_{T'}$ = [**3**] + [**4**] = 3.8(2) × 10^{-3}.

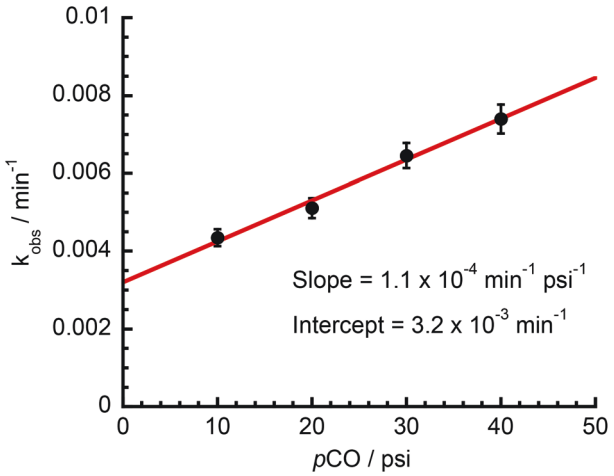

Fig. 3 Plot of k_{obs} for the decay of **3** *versus* CO pressure. Reactions were performed in triplicate in benzene-d_6 with [**3**] = 0.04 M and CO pressures of 10, 20, 30, 40 psi.

The data obtained from Fig. 2 and 3 suggest that **3** reacts *via* two parallel independent pathways. These pathways can be expressed by eqn (1) (where k_{iso} = rate constant for isomerization and k_{ins} = rate constant for insertion) and the proposed mechanism depicted in Scheme 6. Complex **3** either reacts with CO directly to produce **4** (insertion), or *via* isomerization *via* distortion of the PNP ligand around the Ar–N–Ar backbone to generate isomer **3′**, which is then trapped by CO (*vide infra*) to afford the intermediate **3′·CO**. The subsequent reaction of intermediate **3′-CO** or **4** with additional equivalents of CO over several hours leads to **5** (*vide infra*).

$$\frac{-\mathrm{d}[\mathbf{3}]}{\mathrm{d}t} = \frac{\mathrm{d}[\mathbf{4}]}{\mathrm{d}t} = [\mathbf{3}](k_{ins}[CO] + k_{iso}). \quad (1)$$

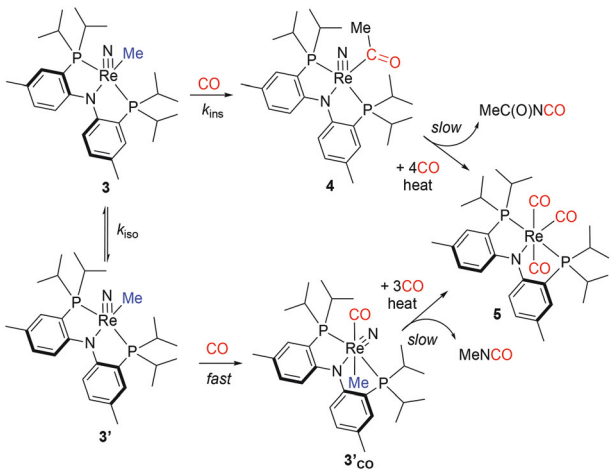

Scheme 6 Proposed mechanisms for the parallel pathways for the carbonylation of **3**.

The rate of isomerization of **3** is given by eqn (2) while the rate of formation of **4** is given by eqn (3).

$$\frac{\mathrm{d}[\mathbf{3'\cdot CO}]}{\mathrm{d}t} = k_{iso}[\mathbf{3}] \quad (2)$$

$$\frac{\mathrm{d}[\mathbf{4}]}{\mathrm{d}t} = k_{ins}[CO][\mathbf{3}]. \quad (3)$$

From eqn (2) and (3) the ratio of [**4**]/[**3′·CO**] is given by eqn (4).

$$\frac{[\mathbf{4}]}{[\mathbf{3'\cdot CO}]} = \frac{k_{ins}[CO]}{k_{iso}}. \quad (4)$$

From the slope and intercept in Fig. 3 and the CO pressure of 20 psi used in Fig. 2, eqn (4) predicts a ratio of [**4**]/[**3′·CO**] of 2 : 3. This is consistent with the data in Fig. 3 and the isolated yield for **4**.

Kinetic simulations[15] were also employed in order to provide further verification for the mechanism in Scheme 6. Rate constants from Fig. 2, and a CO pressure of 20 psi were utilized for this simulation. In addition, rate constants for the formation of **3′·CO** were estimated from DFT calculations (*vide infra*). As shown in Fig. 4, these simulations accurately reproduce the experimental data in Fig. 2, lending support for the mechanism in Scheme 6.

Reaction of 3 with 2,6-dimethylphenyl isocyanide

To gain further insight into the nature of the CO addition pathway, reactions were performed with 2,6-dimethylphenenyl isocyanide, which is isoelectronic with CO. Complex **3** reacts with 2,6-dimethylphenyl-isocyanide to afford the pseudo octahedral complex **6** (Scheme 7). Complex **6** was characterized by

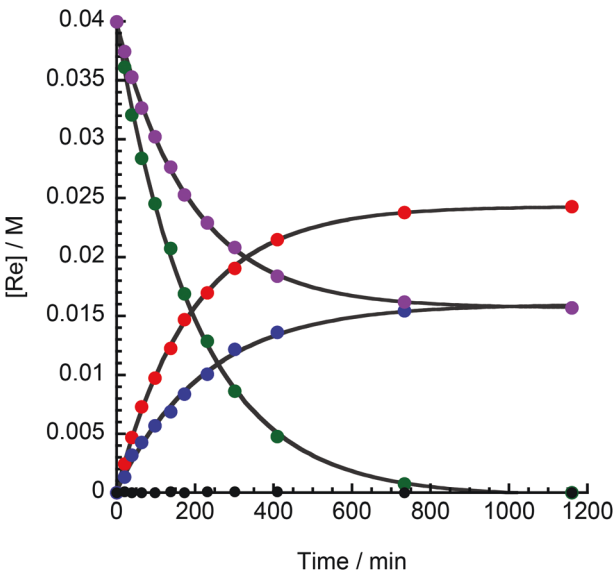

Fig. 4 Kinetic simulations according to the proposed mechanism in Scheme 6. Rate constants were: k_{ins} = 2 × 10^{-3} min^{-1}; k_{iso} = 3 × 10^{-3} min^{-1}; k_5 = 62 mol^{-1} min^{-1}. Legend: [**3**] = green; [**4**] = blue; [**3′·CO**] = red; $[Re]_T$ = [**3**] + [**4**] = purple; [**3′**] = black.

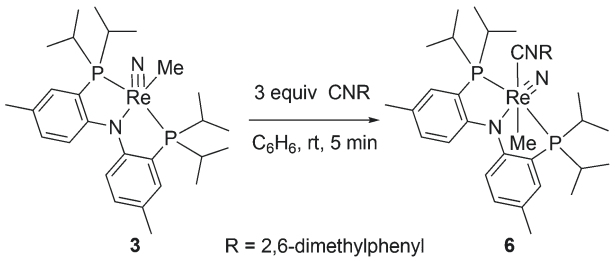

Scheme 7 Synthesis of **6**.

NMR spectroscopy and X-ray crystallography. Insertion of the isocyanide ligand into the Re–Me bond did not occur since the methyl ligand is observed as a triplet at 0.78 ppm with the characteristic coupling to two equivalent phosphorus nuclei. Other resonances are consistent with previously reported PNP complexes.[5f]

X-ray crystal structure of 6

Vapor diffusion of pentane into a concentrated solution of **6** in benzene afforded X-ray quality crystals. The thermal ellipsoid plot of **6** is depicted in Fig. 5. The strong *trans* influence of the nitrido ligand, as well as the steric bulk imposed by the isopropyl groups on the PNP ligand, results in the coordination of the isocyanide group *syn* to the rhenium–nitrido and rhenium–amide bonds. The result of this coordination environment is that the methyl group (C36) is *trans* to the isonitrile carbon (C27) and the nitrido ligand (N2) is *trans* to the amide (N1) bond. The strong *trans* influence of the nitrido ligand substantially elongates the Re1–N1 bond to 2.29 Å, which compared to the corresponding bond in the X-ray structure for **4**, (2.14 Å) is approximately a 7% increase in Re–N bond length observed.

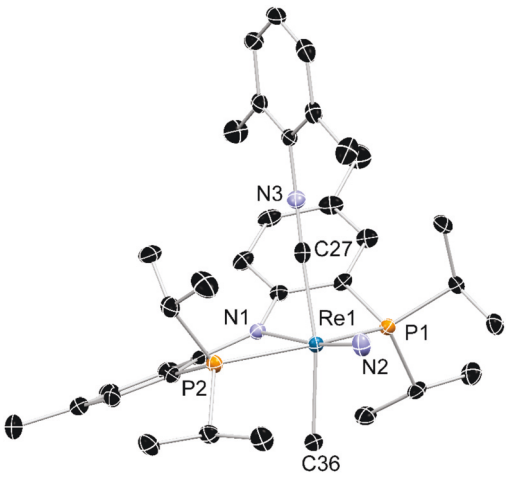

Fig. 5 X-ray crystal structure for **6**. Ellipsoids are at the 50% probability level. Hydrogens are omitted for clarity. Selected bond lengths (Å): Re1–N1 2.289(3); Re1–N2 1.687(2); Re1–C36 2.223(4); Re1–C27 2.046(4); Re1–P1 2.412(0); Re1–P2 2.424(0); C27–N3 1.175(5).

The reactivity of 2,6-dimethylphenyl isocyanide with **3** is complementary to the analogous reaction with CO. The disparate reactivity observed may provide insights into the mechanism for the formation of **5**.

DFT calculations

Insertion of carbon monoxide and methyl isocyanide. In order to gain insights into the mechanism for the reactions of **3** with CO and CNR, DFT(M06)[12] calculations were performed. For simplicity and computational cost, methyl isocyanide was utilized as the isonitrile substrate since isonitriles are isoelectronic with CO.

The free energy diagram describing the insertion of CO and methyl isocyanide is shown in Fig. 6. The strong *trans* influence of the nitrido ligand results in similar insertion mechanisms to related oxo species.[3] Both reactions proceed by initial association of CO/CNR to form the encounter complexes $\mathbf{3_{CO}}$ or $\mathbf{3_{CNR}}$. The Re–CO and Re–CNR bond lengths (2.88 and 2.62 Å) are long which suggests that these species are weakly associated adducts. The long bond lengths and relatively high energies of these two intermediates suggest that these species are transient and proceed directly to the insertion transition states $\mathbf{TS1_{CO}}$ and $\mathbf{TS1_{CNR}}$. The high energy of intermediates $\mathbf{3_{CO}}$ or $\mathbf{3_{CNR}}$ is a direct consequence of the strong *trans* influence of the nitrido ligand, which renders the association of CO or CNMe unfavorable. The difference in the free energies of activation ($\Delta\Delta G^{\ddagger}$) between the transition states for the insertion of CO and CNMe into the Re–Me bond in **3** accounts for the observed difference in reactivity between the two substrates.

As depicted in Fig. 6, the insertion barrier for methyl isocyanide is 3.9 kcal mol^{-1} higher than the corresponding barrier for CO insertion, while the overall reaction is exergonic for both substrates (ΔG° = −12 kcal mol^{-1} and −15 kcal mol^{-1}).

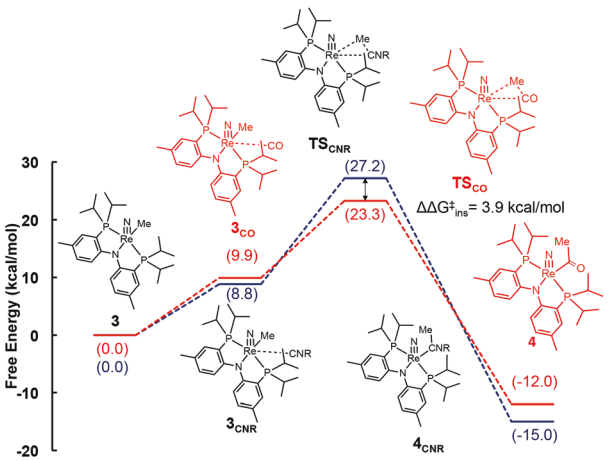

Fig. 6 Calculated Gibbs free energies of transition states and intermediates leading to acyl ($\mathbf{4_{CO}}$) or iminoacyl ($\mathbf{4_{CNR}}$). Computational details: geometry optimization and frequency calculations were carried out with the M06 functional with the 6-31G (d,p) basis set on light atoms and SDD + f basis set on Re. Displayed energies include solvation included *via* the PCM model in benzene and were calculated with the 6-311G++(d,p) basis set on light atoms and SDD + f basis set on rhenium.

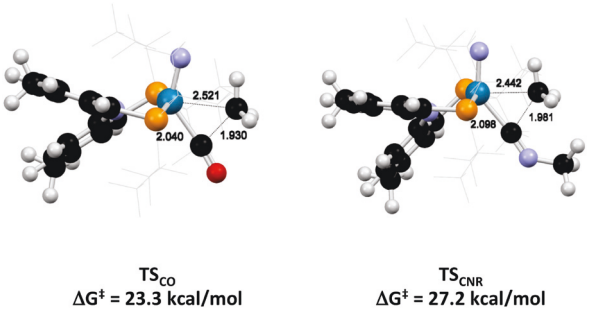

Fig. 7 DFT optimized structures of insertion transition states TS_{CO} (left) and TS_{CNR} (right). Diisopropyl groups of the PNP ligand are displayed in wireframe format for clarity. Legend: nitrogen = purple; rhenium = blue; phosphorus = orange; carbon = black; hydrogen = white.

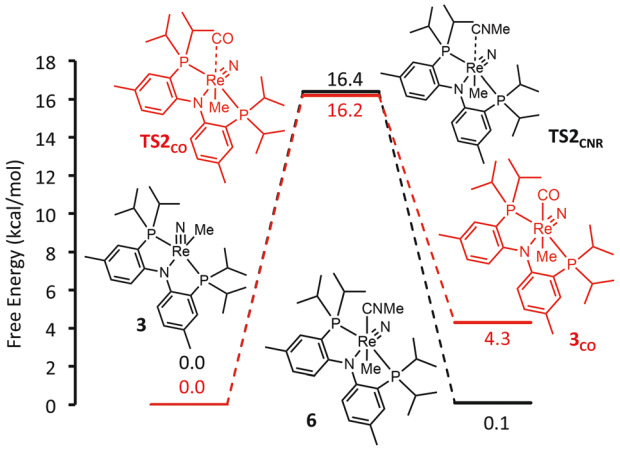

Fig. 8 Calculated Gibbs free energies of transition states and intermediates leading to addition products **6** or $\mathbf{6_{CO}}$. Computational details: Geometry optimization and frequency calculation were carried out with the M06 functional with the 6-31G (d,p) basis set on light atoms and SDD + f basis set on Re. Energies include solvation implemented *via* the PCM model in benzene and calculated with the 6-311G++(d,p) basis set on light atoms and SDD + f basis set on rhenium.

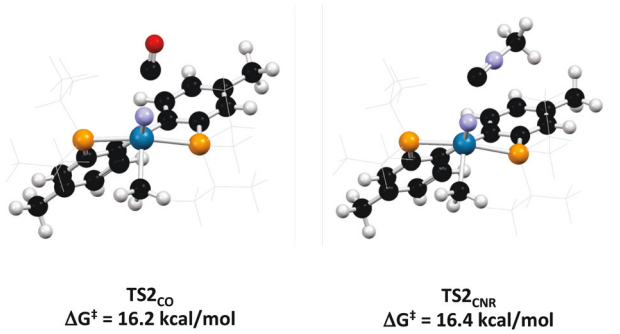

Fig. 9 DFT optimized structures of transitions states leading to coordination of CO or CNR. Diisopropyl groups of the PNP ligand are displayed in wireframe format for clarity. Legend: nitrogen = purple; rhenium = blue; phosphorus = orange; carbon = black; hydrogen = white.

These data are consistent with the experimental observation that while the insertion of CO was observed, the corresponding insertion of 2,6-dimethylphenyl isocyanide did not occur at room temperature. Further, the calculated activation energy for methyl isocyanide (27.2 kcal mol^{-1}) is likely lower than the activation energy for the more sterically encumbered 2,6-dimethylphenyl isocyanide, which was used in experimental studies.

The structures of the insertion transitions states for CO and CNMe are depicted in Fig. 7. The two transition states closely resemble transition states for insertion in previously reported oxorhenium(v) methyl, phenyl and hydride complexes.[3] In both cases, significant elongation of the Re–Me bond is observed, which is consistent with significant bond cleavage. Since isocyanide is a weaker π acceptor than CO, the higher energy of $\mathbf{TS_{CNR}}$ may be attributed to the attenuated stabilization of the transition state *via* the π donation from the metal centered d_{xy} orbital into the antibonding C≡N orbital of the isocyanide ligand.

***Syn* addition of CO/CNR.** The reaction between **3** and 2,6-dimethylphenyl isocyanide to yield **6** proceeds *via* the addition of CNR *syn* to the rhenium amide bond. While this reactivity was not observed in the case of CO, it may account for the formation of **5**. As a result, we carried out DFT studies on the CO/CNR addition *syn* to the Re–N(amide) and Re≡N bonds. The results obtained are depicted in Fig. 8.

The two pathways leading to addition products **6** and $\mathbf{3_{CO}}$ both proceed *via* similar transition states. The barriers are comparable and accessible at room temperature; however, the CO addition product is thermodynamically unfavorable (ΔG° = 4.3 kcal mol^{-1}) and is therefore not observed experimentally. The addition product **6**, on the other hand, is thermoneutral (0.1 kcal mol^{-1}) and consistent with this, additional equivalents of 2,6-dimethylphenyl isocyanide were needed to prevent the loss of the isocyanide ligands in methylene chloride solutions of **6**.

The transition states depicted in Fig. 9 appear to favor substrate approach from the least hindered side of the PNP ligand. In both structures, the positioning of the right ring "up" relieves steric factors by forcing isopropyl groups away from the substrate thus allowing its coordination.

To summarize, the insertion reaction of CO into the Re–Me bond of **3** is observed because the activation energy for insertion (23.3 kcal mol^{-1}) is kinetically accessible at room temperature, whereas the corresponding activation energy for isocyanide insertion (27.2 kcal mol^{-1}) is not. As a result, isocyanide insertion into the Re–Me bond is not observed experimentally. Thus the preference for CO insertion *versus* CNR insertion is kinetic. In contrast, the *syn* addition of CNR to the plane containing the Re–N(amide) and Re≡N bonds is thermoneutral (0.1 kcal), whereas the corresponding reaction with CO is endergonic (4.3 kcal mol^{-1}), and reversible. Thus, the preference for CNR addition compared to CO addition is thermodynamic, and as a result, while **6** was isolated, the corresponding CO addition product was not. More importantly, these data show that the addition CO and CNR to **3** and **3′** is accessible at room temperature. Because CNR is isoelectronic with CO, **6** can be viewed

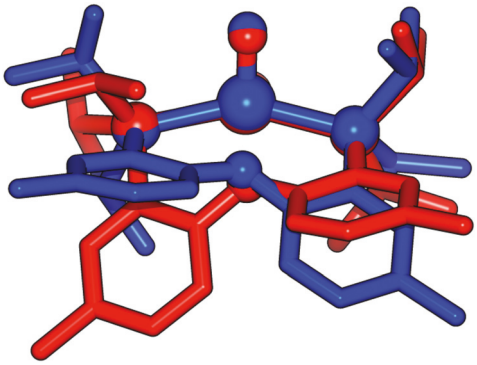

Fig. 10 Overlaid structures for the isomers **3** (red) and **3′** (blue).

as a model for **3′·CO**, which results from the addition of CO to **3′**. However, as described above, both reactions are reversible at room temperature.

Conformational isomerization in 3. The major structural difference between **3** and **3′** involves the torsion angle between two aryl rings linked by the central nitrogen (amide) atom (Fig. 10).

While isomer **3** has a torsion angle of 22.7°, isomer **3′** contains a torsion angle of 31.1°. Since CO insertion into the Re–Me bond requires the approach of CO *trans* to the Re≡N fragment, insertion in **3** is more likely as this isomer provides a less sterically hindered channel for the approach of CO (Fig. 11). There is therefore a much greater preference for the addition of CO *syn* to the Re≡N and Re–N(amide) bonds in **3′** rather than *trans* to the Re≡N bond.

Conformational changes of the flexible PNP ligand backbone (Pathway B) were found to have a significantly lower activation energy (15.6 kcal mol^{-1}) compared to methyl migration (23.3 kcal mol^{-1}). The isomer, **3′**, formed upon isomerization, significantly differs in energy from the starting complex, **3**, 4.4 kcal mol^{-1}. This behavior is likely the result of steric interactions imposed by the isopropyl groups, which renders one isomer slightly less stable upon isomerization (Scheme 8).

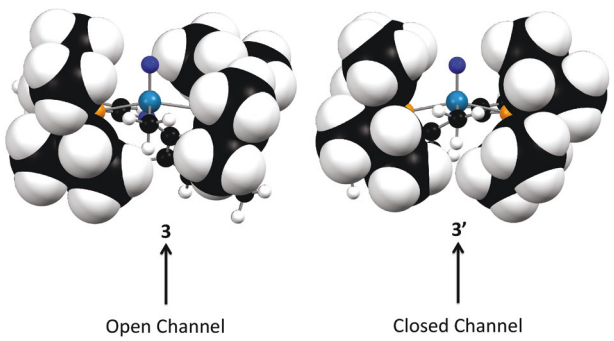

Fig. 11 Calculated structures for two isomers of (PNP)Re(N)Me, **3**. The isopropyl groups are depicted as space-filling models to show channels for the approach of the CO molecule. Legend: nitrogen = purple; rhenium = blue; phosphorus = orange; carbon = black; hydrogen = white.

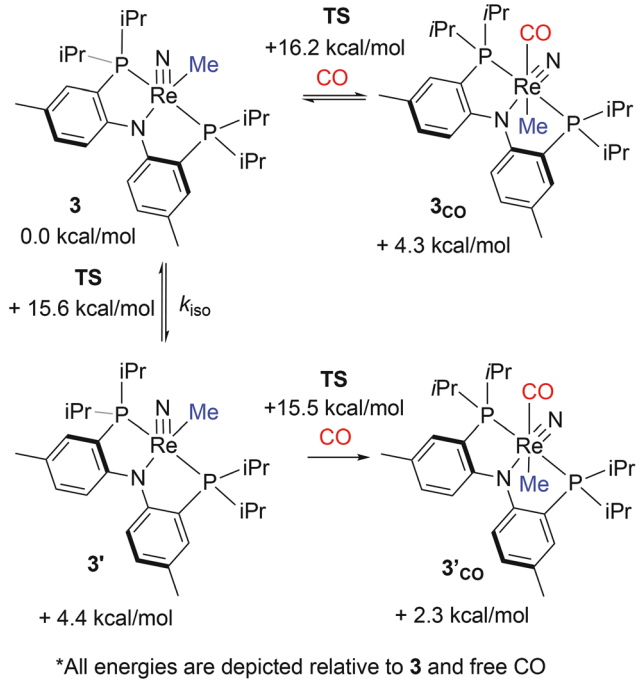

Scheme 8 Relative energies for CO addition *syn* to the Re≡N bond in **3** and **3′**.

While the *syn* coordination of CO to **3** to yield complex (PNP)Re(N)(CO)(Me) is endergonic by 4.3 kcal mol^{-1}, the same reaction with **3′** is exergonic (−2.1 kcal mol^{-1}) with a barrier of 11.1 kcal mol^{-1} (Scheme 8). The low barrier for CO addition to **3′** compared to isomerization is consistent with the experimentally determined rate law. This process makes the CO independent isomerization of the PNP ligand rate limiting, resulting in the observed intercept in Fig. 3 for the overall reaction of **3** with CO.

Release of isocyanate and formation of 5. The volatile and unstable nature of methyl isocyanate makes it difficult to experimentally observe the release of this molecule in the reaction of **3** with CO. Therefore; the reduction of **4** with excess CO was examined. This reaction should lead to the formation of **5** and acetyl isocyanate $CH_3C(O)NCO$, which should be easier to detect *via* spectroscopic methods. The reduction of **4** proceeds quantitatively at 80 °C to yield **5**, along with acetamide, by ^1H NMR spectroscopy (Scheme 9).

While acetyl isocyanate is not detected directly, its intermediacy is implied by the quantitative detection of acetamide,

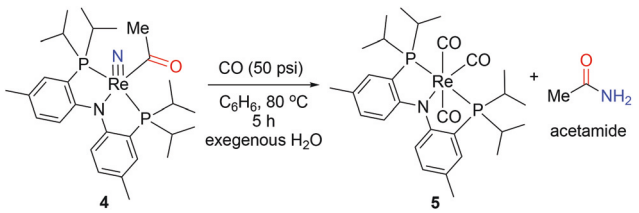

Scheme 9 Reduction of acyl species to tricarbonyl.

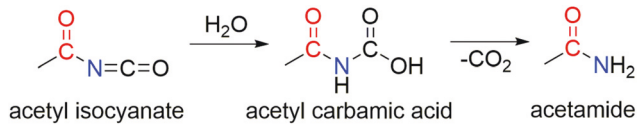

Scheme 10 Decomposition of acetyl isocyanate.

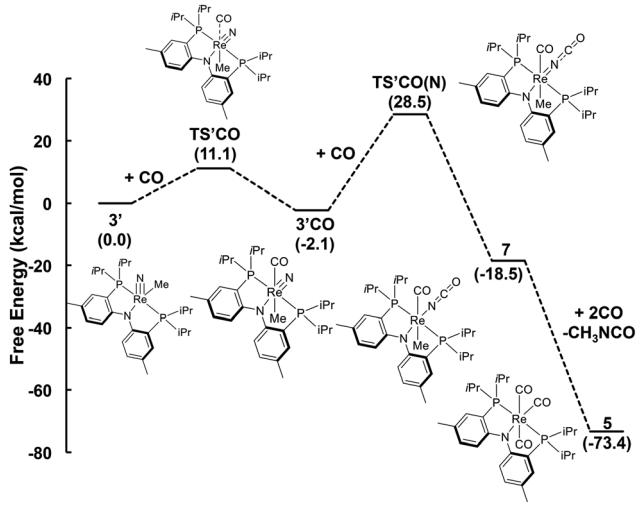

Fig. 12 Calculated free energies leading to isocyanate release and the formation of tricarbonyl complex **5**.

which is formed by rapid trapping of the electrophilic isocyanate by trace amounts of water in solvent, followed by decarboxylation to eliminate CO_2 (Scheme 10).

Methyl isocyanate was likely not detected because of its relative instability in the presence of exogenous water. This reaction would produce methylamine, a gaseous compound that is difficult to detect by spectroscopic methods.

The reduction pathway leading to **5** likely proceeds *via* direct CO attack at the nitrido ligand, to afford **7**, a rhenium (III) isocyanate complex (Fig. 12). This initial reduction is highly exergonic ($\Delta G°$ = −18.5 kcal mol^{-1}) with an activation energy (**TS'CO(N)**) of 28.5 kcal mol^{-1}. The calculated energy is consistent with the observed slow formation of **5** (complex **5** is observed only after heating at 80 °C or at room temperature after several days). Isocyanate release and the formation of **5** are highly exergonic processes with an overall energy of −73.4 kcal mol^{-1}. Although the experimental results are consistent with this pathway and adventitious hydrolysis of released MeNCO, other potential pathways in which free MeNCO is not released cannot be ruled out.

Conclusions

In this manuscript, the synthesis of novel (PNP)Re(N)X (X = Cl and Me) complexes is described. The methylnitridorhenium complex **3** was found to have complementary reactivity with CO and isocyanides, leading to the isolation of a Re(v) acyl complex **4** and an isonitrile adduct **6**. Two parallel pathways were observed for the reaction of **3** with CO: (1) CO inserts into the Re–Me bond to afford **4**, and (2) **3** isomerizes by distortion of the aryl backbone of the PNP ligand to afford the isomer **3′**, this is followed by carbonylation followed by methyl migration to produce **5** and presumably methyl isocyanate.[16,17]

The complementary reactivity of **3** with 2,6-dimethylphenyl isocyanide lends further support for the proposed isomerization pathway. DFT (M06) calculations suggest that insertion of CNR into the Re–Me bond (27.2 kcal mol^{-1}) is inaccessible at room temperature. Instead the substrate adds to the metal center *via* the most accessible face *i.e. syn* to the rhenium-nitrido bond, to afford the isocyanide adduct **6**. The addition of CO to isomer **3′** is proposed to proceed with a similar mechanism to 2,6-dimethylphenyl isocyanide.

This study suggests that like the analogous oxorhenium complexes, carbonylation of rhenium methyl bonds in nitridorhenium complexes is facile. However, it appears that the further tuning of the ligand backbone is necessary in order to prevent the unfavorable decomposition pathways. Ideally, a planar backbone is preferred in the further design of second generation Re(PNP) alkyl complexes in order to prevent unfavorable CO coordination and favor insertion chemistry exclusively.

Experimental section

General considerations

Complex Re(N)(PPh$_3$)$_2$(Cl)$_2$ and the PNP ligand were prepared as previously reported.[2i,7f] All other reagents were purchased from commercial sources and used as received. ^{1}H, ^{13}C, ^{31}P NMR spectra were obtained on 300 or 400 MHz spectrometers at room temperature. Chemical shifts are listed in parts per million (ppm) and referenced to their residual protons or carbons of the deuterated solvents respectively. All reactions were run under an inert atmosphere with dry solvents unless otherwise noted. FTIR spectra were obtained in KBr thin films. Elemental analyses were performed by Atlantic Micro Labs, Inc. Mass Spectrum analysis was carried out on a high resolution mass spectrometer – the Thermo Fisher Scientific Exactive Plus MS, a benchtop full-scan Orbitrap mass spectrometer – using Heated Electrospray Ionization (HESI). The sample was diluted in acetone and analyzed *via* syringe injection into the mass spectrometer at a flow rate of 15 μL min^{-1}. The mass spectrometer was operated in positive ion mode.

General procedure for kinetic data

A solution of **3** (0.04 M) was prepared and aliquots of the solution were transferred into four separate J-Young tubes under N_2 atmosphere in the glove box. The J-Young tubes were degassed *via* three freeze–pump–thaw cycles and were pressurized with CO at various pressures. Reactions were monitored by ^{1}H NMR spectroscopy. Yields were determined with mesitylene as an internal standard.

Computational details

Geometry and transition state optimizations were performed with a 6-31G(d,p)[18] basis set on light atoms and SDD basis set[19] with an added f polarization function on rhenium. Each optimization involved tight optimization criteria implemented in Gaussian 09[20] (opt = tight) with an ultrafine integral grid (int = ultrafine). All structures were fully optimized and analytical frequency calculations were performed on all structures to ensure either a zeroth order saddle point (a local minimum) or a first order saddle point (a transition state). The minima associated with each transition state were determined by animation of the imaginary frequency. Energetics were calculated at 298 K with the 6-311++G(d,p)[21] basis set for C, H, N, O, P atoms and the SDD basis set with an added f polarization function on Re. Reported energies utilized analytical frequencies and the zero point corrections from the gas phase optimized geometries and include solvation corrections which were computed using the PCM method,[22] with benzene as the solvent as implemented in Gaussian 09.

Synthesis of (PNP)Re(N)Cl, 2

Complex $(PPh_3)_2Re(N)Cl_2$ (200 mg, 0.25 mmol) was added to a 25 mL pressure vessel and dissolved in 15 mL of CH_2Cl_2. PNP-H ligand (106 mg, 0.25 mmol, 1 equiv.) was then added to the vessel and the resulting red solution was briefly stirred for 5 min. Anhydrous Et_3N (43 μL, 0.25 mmol) was then added to the mixture and the vessel was heated in 60 °C oil bath for 5 hours. Upon cooling to room temperature, solvent was removed *in vacuo*. The resulting residue was taken up in hexane, filtered, washed with minimal MeOH and dried under vacuum (89 mg isolated, 0.134 mmol, 54% yield). ^{1}H NMR (CH_2Cl_2, 298 K, 300 MHz) δ: 7.43 (d, J = 8.5 Hz, 2H, aryl-H); 7.16 (s, 2H, aryl-H); 6.99 (d, 2H, J = 8.5 Hz, aryl-H); 2.91 (bs, 2H, iPr-H); 2.58 (sp, J = 6.3 Hz, 2H, iPr-H); 2.52 (s, 6H, p-CH_3); 1.45 (overlapping m, 6H, iPr-CH_3); 1.26 (overlapping m, 12H, iPr-CH_3); 0.96 (overlapping m, 6H, iPr-CH_3). ^{31}P NMR (CH_2Cl_2, 298 K, 400 MHz) δ: 51.9 ppm (s). FTIR cm^{-1}: 1079 (Re–N). Elemental analysis: ($C_{26}H_{40}ClN_2P_2Re$) theory (C: 47.02, H: 6.07, N: 4.22) found: (C: 46.72, H: 5.93, N: 4.04). Mass spectrometry (LC-MS): calculated $[M + H]^+$ = 665.19855; experimental $[M + H]^+$ = 665.19668.

Synthesis of (PNP)Re(N)Me, 3

Complex **2** (PNP)Re(N)Cl (200 mg, 0.251 mmol) was added to a 25 ml scintillation vial and dissolved in 15 ml of THF. MeMgBr solution in hexanes (2 equiv., 0.2 ml) was added *via* the syringe and the initially green solution was allowed to reflux for 1 h where it eventually turned red. The resulting red solution was cooled to room temperature. Addition of excess water precipitated the product, which was filtered, washed with hexane and dried *in vacuo* (100 mg isolated, 0.155 mmol, 62% Yield). ^{1}H NMR (CH_2Cl_2, 298 K, 300 MHz). δ: 7.35 (d, J = 8.3 Hz, 2H, aryl-H); 7.08 (s, 2H, aryl-H); 6.93 (d, 2H, J = 8.3 Hz, aryl-H); 2.76 (bs, 2H, iPr-H); 2.52 (sp, J = 6.3 Hz, 2H, iPr-H); 2.27 (s, 6H, p-CH_3); 1.82 (t, J = 4.7 Hz, 3H, Re–Me); 1.39 (overlapping m, 6H, iPr-CH_3); 1.15 (overlapping m, 12H, iPr-CH_3); 0.94 (overlapping m, 6H, iPr-CH_3). ^{31}P NMR (CH_2Cl_2, 298 K, 400 MHz), δ: 54.6 ppm (broad). FTIR cm^{-1}: 1079 (Re–N). Elemental analysis: ($C_{27}H_{43}N_2P_2Re$) theory, (C: 50.37, H: 6.73, N: 4.35); found: (C: 50.37, H: 6.86, N: 4.10). Mass spectrometry (LC-MS): calculated $[M + H]^+$ 645.25317; experimental $[M + H]^+$ = 645.25409.

Synthesis of (PNP)Re(N)(MeC(=O)), 4

Complex **3** (PNP)Re(N)Me (60 mg, 0.155 mmol) was added to a 25 ml pressure vessel and dissolved in 10 ml of benzene. The vessel was degassed using three separate freeze–pump–thaw cycles and pressurized with 40 psi of CO. The solution was heated for 1 h at 80 °C. Upon cooling, all volatiles were then removed *in vacuo* and the resulting solid was treated with excess pentane, filtered and dried *in vacuo*. Recrystallization from benzene/pentane afforded analytically pure complex (40 mg isolated, 63% Yield). ^{1}H NMR (CH_2Cl_2, 298 K, 300 MHz), δ: 7.35 (d, J = 9.1 Hz, 2H, aryl-H) 7.00 (s, 2H, aryl-H), 6.98 (d, 2H, J = 9.1 Hz, aryl-H) 2.95 (s, 3H, Re–C(O)Me) 2.53 (bs, 2H, iPr-H), 2.43 (sp, J = 6.3 Hz, 2H, iPr-H), 2.27 (s, 6H, p-CH_3) 1.35 (overlapping m, 6H, iPr-CH_3), 1.10 (overlapping m, 18H, iPr-CH_3) ^{31}P NMR (CH_2Cl_2, 298 K, 400 MHz) δ: 57.7 (s). FTIR cm^{-1}: 1520 cm^{-1} (CO). Elemental analysis: $C_{28}H_{43}N_2OP_2Re{\cdot}0.5$ (C_6H_6) theory (C: 52.38, H: 6.52, N: 3.94) found (C: 52.42, H: 6.40, N: 3.72).

Synthesis of (PNP)Re(CO)$_3$, 5

In a 25 ml storage tube under an inert atmosphere, $Re(CO)_5Cl$ (84.3 mg, 0.23 mmol) and PNP ligand (100 mg, 0.23 mmol, 1 equiv.) were suspended in benzene. Triethylamine (64 μL, 0.46 mmol, 2 equiv.) was then introduced to the reaction mixture and the resulting yellow solution was allowed to reflux for 1 h. Upon cooling to room temperature, the reaction mixture was filtered through Celite. Removal of solvent under high vacuum with heating at 60 °C afforded (PNP)Re(CO)$_3$ which was recrystallized by slowly evaporating a CH_2Cl_2 solution (82% Yield). ^{1}H NMR (C_6H_6, 298 K, 300 MHz), δ: 7.45 (d, 2H, J = 8.4 Hz, aryl-H) 6.81 (s, 2H, aryl-H) 6.71 (d, 2H, J = 8.4 Hz, aryl-H) 2.17(m. 4H, iPr-H) 2.12 (s, 6H, p-CH_3) 1.04 (m, 24H, iPr-CH_3). ^{31}P (C_6H_6, 298 K, 300 MHz) 44.71 (s). Elemental analysis: $C_{29}H_{40}NO_3P_2Re{\cdot}0.5$ (CH_2Cl_2) theory (C: 47.80, H: 5.58, N: 1.89) found (C: 48.08, H: 5.59, N: 2.08).

Synthesis of (PNP)Re(N)(Me)(2-isocyano-1,3-dimethylbenzene), 6

Complex (PNP)Re(N)Me (25 mg, 0.039 mmol) was added to a 25 ml scintillation vial and taken into the glovebox. 2,6-Dimethylphenyl isocyanide (15.3 mg, 0.117 mmol) was dissolved in benzene and transferred into the vial. The resulting orange mixture was allowed to stir at room temperature for 1 h. Addition of excess pentane resulted in a tan solid, which was filtered, washed with excess pentane and dried under vacuum (13.7 mg isolated, 0.018 mmol, 45% yield). ^{1}H NMR (CH_2Cl_2, 298 K, 300 MHz), δ: 7.10 (bs, 4H, aryl-H), 7.00 (s, 3H, aryl-isocyanide), 6.75 (d, J = 8.5 Hz, 2H, aryl-H), 2.78 (overlap-

ping m, 4H, iPr-H), 2.20 (s, 6H, aryl-CH_3), 2.04 (s, 6H, isocyanide-CH_3), 1.40 (sxt, J = 7.2 Hz, 12 H, iPr-CH_3), 1.25 (q, J = 6.9 Hz, 6H, iPr-CH_3), 1.17 (sxt, J = 7.7 Hz, 6H, iPr-CH_3), 0.78 (t, J = 6.7 Hz, 3H, Re–Me). ^{31}P NMR (CH_2Cl_2, 298 K, 400 MHz) δ: 42.5 (broad multiplet). Satisfactory elemental analysis could not be obtained due to the lability of isocyanide ligand. Mass spectrometry (LC-MS): calculated $[M + H]^+$ = 776.28970; experimental $[M + H]^+$ = 776.32667.

Author contributions

The manuscript was written through contributions of all authors. All authors have given approval to the final version of the manuscript.

Conflicts of interest

The authors declare no competing financial interests.

Acknowledgements

We acknowledge North Carolina State University and the National Science Foundation (CHE-1664973) for funding and the NCSU Office of Information Technology High Performance Computing Services for computational support.

References

1 (*a*) T. A. Fernandes, J. R. Bernardo and A. C. Fernandes, *ChemCatChem*, 2015, **7**, 1177–1183; (*b*) L. Huang, Y. Zhang and H. Wei, *Eur. J. Inorg. Chem.*, 2014, **2014**, 5714–5723; (*c*) P. Gu, W. Wang, Y. Wang and H. Wei, *Organometallics*, 2012, **32**, 47–51; (*d*) Y. Feng, J. Aponte, P. J. Houseworth, P. D. Boyle and E. A. Ison, *Inorg. Chem.*, 2009, **48**, 11058–11066; (*e*) G. Du and M. M. Abu-Omar, *Curr. Org. Chem.*, 2008, **12**, 1185–1198; (*f*) G. Du, P. E. Fanwick and M. M. Abu-Omar, *Inorg. Chim. Acta*, 2008, **361**, 3184–3192; (*g*) E. A. Ison, J. E. Cessarich, N. E. Travia, P. E. Fanwick and M. M. Abu-Omar, *J. Am. Chem. Soc.*, 2007, **129**, 1167–1178; (*h*) E. A. Ison, J. E. Cessarich, G. Du, P. E. Fanwick and M. M. Abu-Omar, *Inorg. Chem.*, 2006, **45**, 2385–2387; (*i*) G. Du and M. M. Abu-Omar, *Organometallics*, 2006, **25**, 4920–4923; (*j*) L. W. Chung, H. G. Lee, Z. Lin and Y.-D. Wu, *J. Org. Chem.*, 2006, **71**, 6000–6009; (*k*) E. A. Ison, R. A. Corbin and M. M. Abu-Omar, *J. Am. Chem. Soc.*, 2005, **127**, 11938–11939; (*l*) E. A. Ison, E. R. Trivedi, R. A. Corbin and M. M. Abu-Omar, *J. Am. Chem. Soc.*, 2005, **127**, 15374–15375; (*m*) K. Ishihara, Y. Furuya and H. Yamamoto, *Angew. Chem.*, 2002, **114**, 3109–3112; (*n*) M. M. Abu-Omar and S. I. Khan, *Inorg. Chem.*, 1998, **37**, 4979–4985; (*o*) W. A. Herrmann, *Angew. Chem., Int. Ed. Engl.*, 1988, **27**, 1297–1313; (*p*) J. C. Bryan, R. E. Stenkamp, T. Tulip and J. M. Mayer, *Inorg. Chem.*, 1987, **26**, 2283–2288.

2 (*a*) A. J. Kosanovich, J. H. Reibenspies and O. V. Ozerov, *Organometallics*, 2016, **35**, 513–519; (*b*) K. Ray, F. Heims, M. Schwalbe and W. Nam, *Curr. Opin. Chem. Biol.*, 2015, **25**, 159–171; (*c*) S. C. Sousa, I. Cabrita and A. C. Fernandes, *Chem. Soc. Rev.*, 2012, **41**, 5641–5653; (*d*) P. M. Reis, P. J. Costa, C. C. Romão, J. A. Fernandes, M. J. Calhorda and B. Royo, *Dalton Trans.*, 2008, 1727–1733; (*e*) G. Du, P. E. Fanwick and M. M. Abu-Omar, *J. Am. Chem. Soc.*, 2007, **129**, 5180–5187; (*f*) B. Royo and C. C. Romão, *J. Mol. Catal. A: Chem.*, 2005, **236**, 107–112; (*g*) B. K. Dirghangi, M. Menon, S. Banerjee and A. Chakravorty, *Inorg. Chem.*, 1997, **36**, 3595–3601; (*h*) A. Neuhaus, A. Veldkamp and G. Frenking, *Inorg. Chem.*, 1994, **33**, 5278–5286; (*i*) B. P. Sullivan, J. C. Brewer, H. B. Gray, D. Linebarrier and J. M. Mayer, *Inorg. Synth.*, 1993, **29**, 146–150; (*j*) W. A. Herrmann, U. Küsthardt, A. Schäfer and E. Herdtweck, *Angew. Chem., Int. Ed. Engl.*, 1986, **25**, 817–818.

3 (*a*) L. K. Robbins, C. P. Lilly, J. L. Smeltz, P. D. Boyle and E. A. Ison, *Organometallics*, 2015, **34**, 3152–3158; (*b*) C. P. Lilly, P. D. Boyle and E. A. Ison, *Organometallics*, 2012, **31**, 4295–4301; (*c*) J. L. Smeltz, C. E. Webster and E. A. Ison, *Organometallics*, 2012, **31**, 4055–4062; (*d*) J. L. Smeltz, P. D. Boyle and E. A. Ison, *J. Am. Chem. Soc.*, 2011, **133**, 13288–13291.

4 (*a*) M. Käß, A. Friedrich, M. Drees and S. Schneider, *Angew. Chem., Int. Ed.*, 2009, **48**, 905–907; (*b*) J. I. van der Vlugt and J. N. Reek, *Angew. Chem., Int. Ed.*, 2009, **48**, 8832–8846; (*c*) D. Benito-Garagorri and K. Kirchner, *Acc. Chem. Res.*, 2008, **41**, 201–213; (*d*) W. Weng, C. Guo, R. Çelenligil-Çetin, B. M. Foxman and O. V. Ozerov, *Chem. Commun.*, 2006, 197–199; (*e*) D. S. McGuinness, P. Wasserscheid, W. Keim, C. Hu, U. Englert, J. T. Dixon and C. Grove, *Chem. Commun.*, 2003, 334–335.

5 (*a*) N. Salvarese, F. Refosco, R. Seraglia, M. Roverso, A. Dolmella and C. Bolzati, *Dalton Trans.*, 2017, **46**, 9180–9191; (*b*) D. Wei, T. Roisnel, C. Darcel, E. Clot and J.-B. Sortais, *ChemCatChem*, 2017, **9**, 80–83; (*c*) M. J. Bezdek and P. J. Chirik, *Angew. Chem., Int. Ed.*, 2016, **55**, 7892–7896; (*d*) I. Klopsch, M. Kinauer, M. Finger, C. Würtele and S. Schneider, *Angew. Chem., Int. Ed.*, 2016, **55**, 4786–4789; (*e*) A. J. Kosanovich, W.-C. Shih, R. Ramirez-Contreras and O. V. Ozerov, *Dalton Trans.*, 2016, **45**, 18532–18540; (*f*) T. J. Korstanje, M. Lutz, J. T. Jastrzebski and R. J. Klein Gebbink, *Organometallics*, 2014, **33**, 2201–2209; (*g*) I. Klopsch, M. Finger, C. Würtele, B. Milde, D. B. Werz and S. Schneider, *J. Am. Chem. Soc.*, 2014, **136**, 6881–6883; (*h*) M. Vogt, A. Nerush, Y. Diskin-Posner, Y. Ben-David and D. Milstein, *Chem. Sci.*, 2014, **5**, 2043–2051; (*i*) M. Vogt, A. Nerush, M. A. Iron, G. Leitus, Y. Diskin-Posner, L. J. W. Shimon, Y. Ben-David and D. Milstein, *J. Am. Chem. Soc.*, 2013, **135**, 17004–17018; (*j*) J. C. DeMott, P. Surawatanawong, S. M. Barnett, C.-H. Chen, B. M. Foxman and O. V. Ozerov, *Dalton Trans.*, 2011, **40**, 11562–11570; (*k*) A. T. Radosevich, J. G. Melnick, S. A. Stoian, D. Bacciu, C.-H. Chen, B. M. Foxman,

O. V. Ozerov and D. G. Nocera, *Inorg. Chem.*, 2009, **48**, 9214–9221; (*l*) A. Choualeb, A. J. Lough and D. G. Gusev, *Organometallics*, 2007, **26**, 3509–3515; (*m*) M. Porchia, F. Tisato, F. Refosco, C. Bolzati, M. Cavazza-Ceccato, G. Bandoli and A. Dolmella, *Inorg. Chem.*, 2005, **44**, 4766–4776; (*n*) O. V. Ozerov, M. Pink, L. A. Watson and K. G. Caulton, *J. Am. Chem. Soc.*, 2004, **126**, 2105–2113; (*o*) O. V. Ozerov, L. A. Watson, M. Pink, M.-H. Baik and K. G. Caulton, *Organometallics*, 2004, **23**, 4934–4943; (*p*) O. V. Ozerov, L. A. Watson, M. Pink and K. G. Caulton, *J. Am. Chem. Soc.*, 2004, **126**, 6363–6378; (*q*) C. Bolzati, F. Refosco, A. Cagnolini, F. Tisato, A. Boschi, A. Duatti, L. Uccelli, A. Dolmella, E. Marotta and M. Tubaro, *Eur. J. Inorg. Chem.*, 2004, **2004**, 1902–1913; (*r*) O. V. Ozerov, L. A. Watson, M. Pink and K. G. Caulton, *J. Am. Chem. Soc.*, 2003, **125**, 9604–9605; (*s*) O. V. Ozerov, J. C. Huffman, L. A. Watson and K. G. Caulton, *Organometallics*, 2003, **22**, 2539–2541.

6 D. E. Herbert and O. V. Ozerov, *Organometallics*, 2011, **30**, 6641–6654.

7 (*a*) H.-W. Suh, T. J. Schmeier, N. Hazari, R. A. Kemp and M. K. Takase, *Organometallics*, 2012, **31**, 8225–8236; (*b*) E. A. Bielinski, P. O. Lagaditis, Y. Zhang, B. Q. Mercado, C. Würtele, W. H. Bernskoetter, N. Hazari and S. Schneider, *J. Am. Chem. Soc.*, 2014, **136**, 10234–10237; (*c*) A. Staubitz, M. E. Sloan, A. P. Robertson, A. Friedrich, S. Schneider, P. J. Gates, J. Schmedt auf der Günne and I. Manners, *J. Am. Chem. Soc.*, 2010, **132**, 13332–13345; (*d*) O. Ozerov, in *The Chemistry of Pincer Compounds*, Elsevier, Amsterdam, 2007, pp. 287–309; (*e*) L.-C. Liang, *Coord. Chem. Rev.*, 2006, **250**, 1152–1177; (*f*) L. Fan, B. M. Foxman and O. V. Ozerov, *Organometallics*, 2004, **23**, 326–328.

8 N. S. Lambic, R. D. Sommer and E. A. Ison, *ACS Catal.*, 2017, **7**, 1170–1180.

9 (*a*) J. Schroer and U. Abram, *Polyhedron*, 2011, **30**, 2157–2161; (*b*) C. C. Romão, F. E. Kühn and W. A. Herrmann, *Chem. Rev.*, 1997, **97**, 3197–3246; (*c*) W. A. Herrmann, M. U. Rauch and G. R. Artus, *Inorg. Chem.*, 1996, **35**, 1988–1991; (*d*) U. Abram and I. Walker, *Acta Crystallogr. Sect. C: Cryst. Struct. Commun.*, 1995, **51**, 1250–1251.

10 (*a*) K. I. Goldberg and R. G. Bergman, *J. Am. Chem. Soc.*, 1989, **111**, 1285–1299; (*b*) G. S. Bodner, A. T. Patton, D. E. Smith, S. Georgiou, W. Tam, W. K. Wong, C. E. Strouse and J. Gladysz, *Organometallics*, 1987, **6**, 1954–1961; (*c*) W. E. Buhro, A. Wong, J. H. Merrifield, G. Y. Lin, A. C. Constable and J. Gladysz, *Organometallics*, 1983, **2**, 1852–1859; (*d*) W. A. Kiel, G. Y. Lin, A. G. Constable, F. B. McCormick, C. E. Strouse, O. Eisenstein and J. Gladysz, *J. Am. Chem. Soc.*, 1982, **104**, 4865–4878.

11 J. L. Smeltz, C. P. Lilly, P. D. Boyle and E. A. Ison, *J. Am. Chem. Soc.*, 2013, **135**, 9433–9441.

12 Y. Zhao and D. G. Truhlar, *Theor. Chem. Acc.*, 2008, **120**, 215–241.

13 See Experimental section and the ESI† for full computational details.

14 R. H. Crabtree, *The Organometallic Chemistry of the Transition Metals*, John Wiley & Sons, 6th edn, 2009.

15 W. Hinsberg and F. Houle, Kinetiscope: a stochastic kinetics simulator http: //hinsberg.net/kinetiscope/(accessed Apr 1, 2017).

16 J. S. Silvia and C. C. Cummins, *J. Am. Chem. Soc.*, 2008, **131**, 446–447.

17 (*a*) A. F. Cozzolino, J. S. Silvia, N. Lopez and C. C. Cummins, *Dalton Trans.*, 2014, **43**, 4639–4652; (*b*) B. L. Tran, M. Pink, X. Gao, H. Park and D. J. Mindiola, *J. Am. Chem. Soc.*, 2010, **132**, 1458–1459; (*c*) B. Askevold, J. T. Nieto, S. Tussupbayev, M. Diefenbach, E. Herdtweck, M. C. Holthausen and S. Schneider, *Nat. Chem.*, 2011, **3**, 532–537.

18 V. A. Rassolov, M. A. Ratner, J. A. Pople, P. C. Redfern and L. A. Curtiss, *J. Comput. Chem.*, 2001, **22**, 976–984.

19 (*a*) M. Dolg, H. Stoll, H. Preuss and R. M. Pitzer, *J. Phys. Chem.*, 1993, **97**, 5852–5859; (*b*) A. Bergner, M. Dolg, W. Küchle, H. Stoll and H. Preuß, *Mol. Phys.*, 1993, **80**, 1431–1441; (*c*) M. Kaupp, P. v. R. Schleyer, H. Stoll and H. Preuss, *J. Chem. Phys.*, 1991, **94**, 1360–1366; (*d*) T. Dunning Jr. and P. J. Hay, in *Modern Theoretical Chemistry*, ed. H. Schaefer III, Plenum, New York, 1977, vol. 3.

20 M. J. Frisch, G. W. Trucks, H. B. Schlegel, G. E. Scuseria, M. A. Robb, J. R. Cheeseman, G. Scalmani, V. Barone, B. Mennucci, G. A. Petersson, H. Nakatsuji, M. Caricato, X. Li, H. P. Hratchian, A. F. Izmaylov, J. Bloino, G. Zheng, J. L. Sonnenberg, M. Hada, M. Ehara, K. Toyota, R. Fukuda, J. Hasegawa, M. Ishida, T. Nakajima, Y. Honda, O. Kitao, H. Nakai, T. Vreven, J. A. Montgomery Jr., J. E. Peralta, F. Ogliaro, M. Bearpark, J. J. Heyd, E. Brothers, K. N. Kudin, V. N. Staroverov, R. Kobayashi, J. Normand, K. Raghavachari, A. Rendell, J. C. Burant, S. S. Iyengar, J. Tomasi, M. Cossi, N. Rega, M. J. Millam, M. Klene, J. E. Knox, J. B. Cross, V. Bakken, C. Adamo, J. Jaramillo, R. Gomperts, R. E. Stratmann, O. Yazyev, A. J. Austin, R. Cammi, C. Pomelli, J. W. Ochterski, R. L. Martin, K. Morokuma, V. G. Zakrzewski, G. A. Voth, P. Salvador, J. J. Dannenberg, S. Dapprich, A. D. Daniels, Ö. Farkas, J. B. Foresman, J. V. Ortiz, J. Cioslowski, D. J. Fox, *Gaussian 09, Revision D.01*, Gaussian, Inc., Wallingford CT, 2009.

21 K. Frick, U. Ziener and M. Hanack, *Eur. J. Inorg. Chem.*, 1999, **1999**, 1309–1313.

22 J. Tomasi, B. Mennucci and E. Cances, *J. Mol. Struct. (THEOCHEM)*, 1999, **464**, 211–226.